

Probing the universe with the Lyman-alpha forest: II. The column density distribution

Nickolay Y. Gnedin

Department of Astronomy, University of California, Berkeley, CA 94720

E-mail: gnedin@astron.berkeley.edu; http://astron.berkeley.edu/~gnedin

17 June 2021

ABSTRACT

I apply the well controlled Hydro-PM approximation of Gnedin & Hui to model the column density distribution of the Lyman-alpha forest for 25 different flat cosmological scenarios, including variants of the standard CDM, tilted CDM, CDM with a cosmological constant, and CHDM models. I show that within the accuracy of the HPM approximation the slope of the column density distribution reflects the degree of nonlinearity of the cosmic gas distribution and is a function of the rms linear density fluctuation at the characteristic filtering scale only. The amplitude of the column density distribution, expressed as the value for the ionizing intensity, is derived as a function of the cosmological parameters (to about 40% accuracy). The observational data are currently consistent with the value for the ionizing intensity being constant in the redshift interval $z \sim 2 - 4$.

Key words: cosmology: theory — intergalactic medium — quasars: absorption lines
– methods: numerical – hydrodynamics

1 INTRODUCTION

Recent years witnessed a rapid development in our understanding of the Lyman-alpha forest, a phenomenon, potentially offering cosmologists the most accurate probe of the Intergalactic Medium (IGM) at intermediate cosmological redshifts ($z \sim 2 - 4$). On one hand, observations with the Keck telescopes (see, for example, Hu et al. 1995; Lu et al. 1996; Cristiani et al. 1996; Kirkman & Tytler 1997; Kim et al. 1997; and D’Odorico et al. 1997) provided an impressive amount of high quality data. On the other hand, cosmological hydrodynamic simulations (Cen et al. 1994; Zhang, Anninos, & Norman 1995; Hernquist et al. 1996; Miralda-Escudé et al. 1996; Wadsley & Bond 1997; Zhang et al. 1997) offered a theory whose *a priori* predictions can now not only be quantitatively compared to the observational data, but also, and perhaps even more importantly, be used to constraint the cosmology with the Lyman-alpha forest observations.

While a possibility still remains that the true nature of the Lyman-alpha is still uncovered, or that there exist a genuine population of individual absorbers (Bahcall & Salpeter 1965; Arons 1972; Black 1981; Ostriker & Ikeuchi 1983; Ikeuchi & Ostriker 1986; Rees 1986; Ikeuchi 1986; Rees 1988; Bond, Szalay, & Silk 1988), this paper is solely based on the theory that Lyman-alpha absorption arises from the fluctuating IGM, and the fluctuations in the IGM are small-scale siblings of larger-scale structures, that one sees in the

distribution of galaxies in the sky, as argued for by cosmological hydrodynamic simulations.

However, cosmological hydrodynamic simulations may be the worst theoretical tool one can imagine. They require enormous (compared to the vast majority of theoretical methods) computational resources, and at the same time demand high expertise from a researcher, who ought to understand a vast number of subtle numerical and modeling biases arising from using such a complicated tool as a cosmological hydrodynamic code. The development of the code takes months, if not years, of human labor, and currently there exist only a few groups who engage in modeling the Lyman-alpha forest with hydrodynamic simulations. This situation will change in the future, when supercomputers are faster and more widely available, and when standard hydrodynamic codes become publicly accessible, but the current situation vows for the use of approximate methods, which sacrifice the accuracy for the sake of simplicity and speed. The simplicity and speed are especially important because currently there exist a large variety of cosmological models that need to be tested against the observational data; while one or two specific cosmological models can be best studied with the hydrodynamic simulations, it is currently beyond reason to investigate dozens of models with the hydrodynamic simulations.

Up to date, two different approximations have been used for the purpose of modeling the Lyman-alpha forest: the log-normal approximation (Bi, Börner & Chu 1992; Gnedin &

arXiv:astro-ph/9706286v2 29 Jan 1998

Hui 1996; Bi & Davidsen 1997) and the Zel’dovich approximation (Doroshkevich, & Shandarin 1977; McGill 1990; Hui, Gnedin, & Zhang 1997). While both approximations are very efficient and much easier to implement than a cosmological hydrodynamic simulation, they are *uncontrolled* approximations, i.e. the range of their applicability and their accuracy is not well established. As a result, their predictions cannot be directly used in a quantitative comparison with the observational data, since it is not clear what the error is to assign to the theoretical prediction based on an approximation (since an approximation is used, it has to have an error associated with it).

In this paper I use a different approximation, called HPM, and developed in Gnedin & Hui (1998). In its essence, the HPM method uses a simple Particle-Mesh (PM) solver modified to account for the effect of gas pressure. Because there exist a tight correlation between gas temperature/pressure and gas density (“equation of state”) in the low density IGM in the mildly nonlinear regime (cosmic overdensity $\delta \lesssim 10$), it is possible to compute the gas temperature and pressure at every point directly from the value of the cosmic gas density at this point. Thus, there is no need to introduce a special equation for the gas temperature as in a full hydrodynamic solver. As a result, the HPM approximation is only about 25% slower (due to the overhead of computing the equation of state) than a simple PM solver, and substantially faster than a full hydrodynamic solver (due to both fewer computations at each time-step and fewer time-steps), while delivering results which are accurate to about 15% in the point-by-point comparison with a full hydrodynamic simulation of precisely the same cosmological model (for $\delta \lesssim 10$).

Standard (i.e. unmodified to account for the gas pressure) PM simulations have been also used to address properties of the Lyman-alpha forest (Petitjean, Mücke & Kates 1995; Mücke et al. 1996; Weinberg 1997). While PM simulations are most likely more accurate than lognormal or Zel’dovich approximations, they still cannot quite reach the level of accuracy achieved by the HPM method. For example, as has been shown by Gnedin & Hui (1998), a standard PM simulation predicts about a factor of 3 lower densities than the full hydrodynamic simulation; it is possible to improve upon the PM simulation by appropriate smoothing of the initial conditions, but even in this case a PM simulation is only able to reproduce the gas density to about 30-40% for $\delta \lesssim 10$, whereas HPM reaches a 15% accuracy.

In general, it does not seem to be much rationale in using the standard PM simulation instead of HPM, because 25% increase in the CPU time in the HPM approach compared to simple PM buys at least a factor of 2 in the error reduction. Also, from a technical point of view, it does not require much human effort to convert a PM code into an HPM code.

Having chosen the tool to study the Lyman-alpha forest, it is most natural to start with investigating the column density distribution, since it is the quantity best known observationally (to within about 10-15%). Since the main advantage of using the HPM approximation is its speed, I concentrate in this paper on analysing the properties of the column density distribution of the Lyman-alpha forest for a large set of different cosmological models (25 altogether) with the main goal to understand what physical parameters

the column density distribution depends upon. Testing of specific cosmological models is only a secondary goal of this paper.

I begin my analysis with discussing the models and characteristic scales in Section 2. In the same section I also discuss another approximation I have to adopt to conclude my study, and carefully investigate the total error induced by using approximations rather than an exact method (in this case a cosmological hydrodynamic simulation). The results are presented in Section 3, and Section 4 concludes the paper with the discussion.

2 METHOD

2.1 Cosmological models

With the help of HPM, it is possible to simulate a large set of cosmological models with only modest computational resources. Table 1 lists all 25 simulations considered in this paper. Simulations have been performed with 256^3 particles on a 256^3 mesh. An average 256^3 simulation takes about 40 CPU-hours on a R10K processor. In addition, 4 simulations have been rerun with 512^3 particles on a 512^3 mesh, to verify numerical convergence. Those four models are shown in bold face in Table 1. Each of 512^3 simulations requires about 450 CPU-hours on a R10K processor, and it is impractical at the moment to perform all simulations listed in Table 1 with the 512^3 mesh. I therefore use the 512^3 simulations to investigate numerical convergence and accuracy of the results obtained with 256^3 models.

Placement of a simulation box has been chosen so as to insure that the characteristic scale over which linear baryon fluctuations are smoothed, the so called *filtering scale* (Gnedin & Hui 1998), is resolved with at least 3 cells. This dictates the comoving cell size of $10h^{-1}$ kpc for $\Omega_0 = 1$ models and $15h^{-1}$ kpc for LCDM models, with the exception of the SCDM.2K and SCDM.2L models, whose low reionization temperature and late reionization (and therefore a small filtering scale) required to use the cell size of $7h^{-1}$ kpc.

Cosmological parameters and labels for all models are summarized in Table 1. Here Ω_0 is the total matter density parameter, Ω_b is the baryon density parameter, Ω_Λ is the cosmological constant density parameter, and Ω_ν is the density parameter in massive neutrinos. As usual, h denotes the Hubble constant in units of 100 km/s/Mpc, n is the power-law index of the primordial spectrum of density fluctuations ($n = 1$ is the scale-free Harrison-Zel’dovich spectrum), and σ_8 is the rms top-hat density fluctuation on $8h^{-1}$ Mpc at $z = 0$,

$$\sigma_8^2 \equiv \int_0^\infty \frac{k^2 dk}{2\pi^2} P(k) W_{\text{TH}}^2(k \times 8h^{-1} \text{ Mpc}).$$

In order to simulate the evolution of the IGM under the HPM approximation, an equation of state (i.e. the temperature-density relation) as a function of time ought to be specified. In general, the equation of state depends on the time evolution and spectral shape of the ionizing background, which is a two-dimensional function. In order to limit the possible choice of time-dependent equations of state to a manageable set, I adopt the power-law equation of state in the form derived in Hui & Gnedin (1998),

Table 1. Cosmological Models

Model	Ω_0	Ω_b	Ω_Λ	Ω_ν	h	n	σ_8	σ_{34}	$T_{4,\text{rei}}$	z_{rei}	γ	T_4	σ_F	$\sigma_{F,\text{BOX}}$	COBE
SCDM.1A	1	0.05	0	0	0.5	1	0.8	2.22	2.5	7	1.49	0.91	2.39	2.15	
SCDM.2A	1	0.05	0	0	0.5	1	0.7	1.95	2.5	7	1.49	0.91	2.09	1.88/2.00	
SCDM.2D^a	1	0.05	0	0	0.5	1	0.7	1.95	2.5	7	1.49	0.91	2.09	1.88/2.00	
SCDM.2E ^a	1	0.05	0	0	0.5	1	0.7	1.95	2.5	7	1.49	0.91	2.09	1.88	
SCDM.2G	1	0.05	0	0	0.5	1	0.7	1.95	1.5	7	1.51	0.61	2.23	2.04	
SCDM.2H	1	0.05	0	0	0.5	1	0.7	1.95	4.0	7	1.46	1.32	1.96	1.74	
SCDM.2J	1	0.05	0	0	0.5	1	0.7	1.95	2.5	15	1.61	0.74	1.92	1.70	
SCDM.2L	1	0.05	0	0	0.5	1	0.7	1.95	2.5	5	1.33	1.21	2.26	2.00	
SCDM.3A	1	0.05	0	0	0.5	1	0.6	1.67	2.5	7	1.49	0.91	1.79	1.62	
SCDM.4A	1	0.05	0	0	0.5	1	0.5	1.39	2.5	7	1.49	0.91	1.49	1.35/1.43	
SCDM.5A	1	0.05	0	0	0.5	1	1.2	3.34	2.5	7	1.49	0.91	3.58	3.23/3.52	✓
TCDM.2A	1	0.05	0	0	0.5	0.9	0.83	1.95	2.5	7	1.49	0.91	2.09	1.84	✓
TCDM.4A	1	0.05	0	0	0.5	0.7	1.16	1.95	2.5	7	1.49	0.91	2.10	1.74	
LCDM.1A	0.35	0.05	0.65	0	0.7	1	0.94	1.85	2.5	7	1.53	1.25	1.94	1.69	✓
LCDM.1C	0.35	0.05	0.65	0	0.7	1	0.94	1.85	1.5	5	1.43	0.96	2.26	2.06	✓
LCDM.2A	0.35	0.05	0.65	0	0.7	0.96	0.80	1.49	1.5	5	1.43	0.96	1.80	1.62	✓
LCDM.3A	0.35	0.03	0.65	0	0.7	1	1.04	2.14	2.5	7	1.51	1.02	2.27	2.01	✓
LCDM.4A	0.35	0.03	0.65	0	0.7	0.95	0.85	1.62	2.5	7	1.51	1.02	1.72	1.50	✓
LCDM.5A	0.4	0.036	0.6	0	0.65	1	1.02	2.12	2.5	7	1.51	1.04	2.25	2.00	✓
CHDM.1A	1	0.05	0	0.1	0.5	1	0.91	2.13	2.5	7	1.49	0.91	2.26	2.02	✓
CHDM.2A	1	0.05	0	0.15	0.5	1	0.85	1.69	2.5	7	1.49	0.91	1.78	1.57	✓
CHDM.3A	1	0.05	0	0.2	0.5	1	0.81	1.35	2.5	7	1.49	0.91	1.41	1.22	✓
CHDM.4A	1	0.05	0	0.1	0.65	1	1.21	3.29	2.5	7	1.50	0.99	3.46	3.12	✓
CHDM.5A	1	0.05	0	0.2	0.65	1	1.11	2.10	2.5	7	1.50	0.99	2.19	1.89	✓
CHDM.6A	1	0.07	0	0.1	0.6	0.9	0.72	1.55	2.5	7	1.52	1.09	1.61	1.41	✓

^a A different random realization of the SCDM.2A model.

$$T(\rho) = T_0(1 + \delta)^{\gamma-1}, \quad (1)$$

where δ is the cosmic overdensity, and T_0 and γ are functions of redshift. Specifically, I adopt the evolution of T_0 and γ from Hui & Gnedin (1998), equations (17) and (19). In this case the evolution of the equation of state is determined by only two parameters, the epoch of sudden reionization z_{rei} , and the temperature of the gas just after reionization, T_{rei} . Those two parameters are shown in Table 1 for all models, with the reionization temperature expressed in units of 10^4 K,

$$T_{4,\text{rei}} \equiv T_{\text{rei}}/10^4 \text{ K},$$

with reasonable values ranging from $T_{4,\text{rei}} \sim 1$ to $T_{4,\text{rei}} \sim 4$. For the purpose of this paper it is only important that equation (1) gives an equation of state, and by changing parameters T_{rei} and z_{rei} I can span a reasonable range in possible equations of state. As will be shown below, the specific form of the equation of state plays a relatively minor role in determining the column density distribution of the Lyman-alpha forest.

Given the specific form of the evolution of the equation of state, it is then possible to compute the filtering scale as a function of redshift for a given cosmological model. In general, the wavenumber k_F corresponding to the filtering scale is given by the following expression (Gnedin & Hui 1998):

$$\frac{1}{k_F^2(t)} = \frac{1}{D_+(t)} \int_0^t dt' a^2(t') \frac{\ddot{D}_+(t') + 2H(t')\dot{D}_+(t')}{k_J^2(t')}$$

$$\int_{t'}^t \frac{dt''}{a^2(t'')}, \quad (2)$$

where $D_+(t)$ is the growing mode of linear fluctuations, and

$$k_J \equiv \frac{a}{c_S} \sqrt{4\pi G \bar{\rho}} \quad (3)$$

is the wavenumber corresponding to the Jeans scale. Here c_S is the sound speed of the cosmic gas, and $\bar{\rho}$ is the total cosmic mean density. For the fully ionized cosmic gas with the mean molecular weight $\mu = 0.6$ and with the equation of state given by (1), k_J can be expressed as

$$k_J(z) = 8.44 \Omega^{1/2} h \text{ Mpc}^{-1} \left(\frac{1.5(1+z)}{\gamma T_4} \right)^{1/2}, \quad (4)$$

where $T_4 \equiv T_0/10^4$ K. In general, the filtering scale is a complicated function of time, but for a large set of reasonable equations of state it is about a half of the Jeans scale at $z \sim 3$, $k_F \sim 2k_J$. It is therefore useful to introduce a measure of nonlinearity of the gas distribution of a given cosmological model at $z = 3$, σ_{34} , defined as

$$\sigma_{34}^2 \equiv \int_0^\infty \frac{k^2 dk}{2\pi^2} P(k, z=3) \exp(-2k^2/k_{34}^2), \quad (5)$$

where

$$k_{34} \equiv 34 \Omega_0^{1/2} h \text{ Mpc}^{-1} \quad (6)$$

is the wavenumber corresponding to one half of the Jeans scale for the cosmic gas with $T_4 = 1$ and $\gamma = 1.5$ at $z = 3$. The particular choice of filtering was discussed in Gnedin & Hui (1998). The quantity σ_{34} should therefore indicate an

approximate degree of nonlinearity of the gas distribution in a given cosmological model at $z \approx 3$. A more accurate indicator is of course the rms linear density fluctuation at the filtering scale,

$$\sigma_F^2(z) \equiv \int_0^\infty \frac{k^2 dk}{2\pi^2} P(k, z) \exp[-2k^2/k_F^2(z)], \quad (7)$$

and $k_F(z)$ is a function of time. While σ_F is a more accurate measure, it is also more difficult to compute (since it requires evaluation of k_F). On the other hand, σ_{34} is less accurate but easier to compute, and it can be useful for quick, order-of-magnitude estimates.

Since a simulation is performed on a finite box, only a finite range of scales is present in the simulation. Thus, the rms density fluctuation computed in a simulation will be smaller than the one obtained using the full range of scales. To be able to account for this effect, I introduce another quantity, $\sigma_{F,\text{BOX}}$, similar to equation (7), but with integration performed over only a finite range of scales from k_{min} to k_{max} which are present in the simulation box:

$$\sigma_{F,\text{BOX}}^2(z) \equiv \int_{k_{\text{min}}}^{k_{\text{max}}} \frac{k^2 dk}{2\pi^2} P(k, z) \exp[-2k^2/k_F^2(z)], \quad (8)$$

The small scale cut-off, k_{max} , is not that important because the exponential filtering insures that, as long as the filtering scale $1/k_F$ is resolved with at least three cell sizes ($k_F < 1/(3l)$ where l is the cell size), any contribution to the integral at $k \sim k_{\text{max}} \equiv \pi/l$ (the Nyquist frequency) is suppressed by a factor $\exp[-2(3\pi)^2]$, which is equal zero for any practical purpose.

Values of σ_{34} , $\sigma_F(z = 2.85)$, and $\sigma_{F,\text{BOX}}(z = 2.85)$ are shown in Table 1 (for four models for which both 256^3 and 512^3 simulations have been run, both values of $\sigma_{F,\text{BOX}}(z = 2.85)$ are shown). Also, for reference purposes, I show values for T_4 and γ which define the equation of state of the IGM at $z = 2.85$. The redshift value of $z = 2.85$ corresponds to the epoch where most abundant observation data on the column density distribution exist (Hu et al. 1995; Kirkman & Tytler 1997; Kim et al. 1997). The check mark in the last column of Table 1 indicates whether a particular model is *COBE* normalized. The *COBE* normalization was done using Bunn & White (1997) fits and assuming the gravity wave contribution for $n < 1$ models.

In order to specify initial conditions for a simulation, a linear matter transfer function needs to be computed. For my LCDM simulations I used transfer functions computed using the linear gravity code (existing in the literature fits are not sufficiently accurate due to the higher baryonic fraction in LCDM models compared to $\Omega_0 = 1$ models); Hu & Sugiyama (1996) approximation was used to compute transfer functions for SCDM and TCDM simulations, and Ma (1996) fits were used for CHDM simulations.

Finally, a few words about the choice of models. Apparently, only *COBE* normalized models can be considered viable. The set of SCDM models, which are not *COBE* normalized, is therefore used as a kind of “training set”, with which dependence on different parameters is analysed in order to develop a general understanding of how the column density distribution of the Lyman-alpha forest depends on the underlying cosmology.

2.2 The column density distribution

The purpose of this paper is to investigate the column density distribution of the Lyman-alpha forest, and I therefore need a way to compute the column density distribution from the output of a simulation. The standard way of accomplishing this is to generate synthetic spectra and then fit Voigt profiles (Dave et al. 1997). However, the Voigt profile fitting is extremely CPU intensive, and full Voigt profile analysis of results of one simulation would require more computer time than the simulation itself consumed. It is therefore feasible to use an approximate technique and then properly account for the error induced.

Fortunately, there is such an approximate method called the “Density-Peak Ansatz” (hereafter DPA), introduced in (Gnedin & Hui 1996; Hui, Gnedin, & Zhang 1997). The DPA approximation is based on the assumption that a single Lyman-alpha line arises from a peak in the cosmic gas density along the line of sight to a distant quasar. Then, given the value of the cosmic density $\rho \equiv 1 + \delta$ at the peak, and the second derivative of the density along the line of sight (the first derivative vanishes at the peak), a value for the column density can be associated with the peak as follows:

$$N_{\text{H I}} \equiv 1.45 \times 10^{13} \text{ cm}^{-2} T_4^{-0.7} \left(\frac{\Omega_b h^2}{0.0125} \right)^2 \left(\frac{0.5}{J_{21}} \right) \left(\frac{1+z}{4} \right)^5 \\ (1+\delta)^{2-0.7(\gamma-1)} \left[-(1-0.35(\gamma-1)) \frac{d^2 \ln(1+\delta)}{dx^2} \right]^{-1/2}, \quad (9)$$

and x being measured in Mpc. Here J_{21} is the ionizing intensity,

$$J_{21} \equiv \frac{\int J_\nu \sigma_\nu d\nu/\nu}{\int \sigma_\nu d\nu/\nu} \times \frac{1}{10^{-21} \text{ erg cm}^{-2} \text{ s}^{-1} \text{ Hz}^{-1} \text{ sr}^{-1}},$$

where J_ν is the radiation intensity and σ_ν is the hydrogen photoionization cross-section.

In order to test the DPA approximation, I have computed synthetic spectra for random lines of sight through the simulation box for several models at $z = 2.85$ and fitted Voigt profiles to Lyman-alpha forest lines using AUTOVP automatic Voigt profile fitting code (Dave et al. 1997), kindly provided to me by Romeel Dave. In order to do that, I need to assume a value for the ionizing intensity J_{21} , and also specify the signal-to-noise ratio S/N for Voigt profile fitting (the DPA column densities are independent of the adopted signal-to-noise ratio). Figure 1 shows the scatter plot of column densities from the DPA approximation versus column densities computed using Voigt profile fitting for the SCDM.2A model assuming $J_{21} = 0.17$ (which gives a reasonable fit to the observational data from Hu et al. 1995) and $S/N = 50$. Note, that while there are absorption lines on which the DPA approximation fails severely, in large the agreement is remarkable, keeping in mind the simplicity of the DPA method.

Column density distributions from the DPA method and Voigt profile fitting for several models are shown in Figure 2 with thin and bold lines respectively. The solid line shows the SCDM.2A model with $J_{21} = 0.17$ and $S/N = 50$, while the dotted line shows the same model but with $S/N = 100$. I also show the CHDM.3A and LCDM.3A models on the same plot, as well as the SCDM.2A model at $z = 3.70$.

One can see that DPA agrees very well (to about 3%)

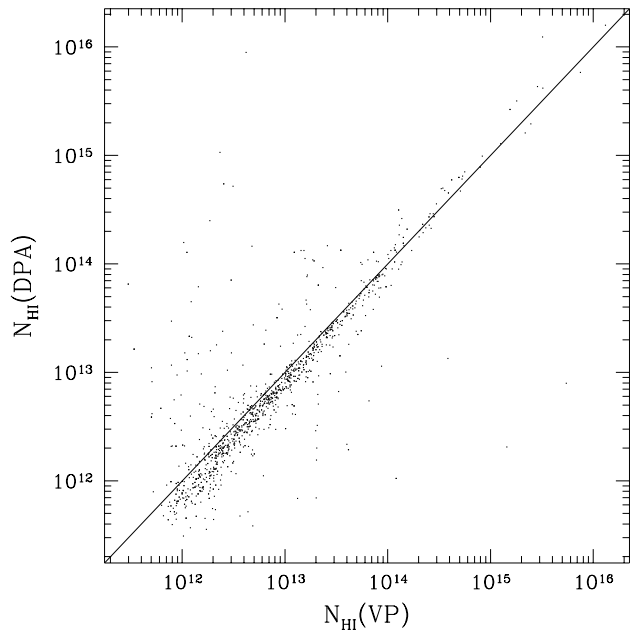


Figure 1. Scatter plot of column densities computed using the DPA approximation vs column densities obtained by Voigt profile fitting for the SCDM.2A model with $J_{21} = 0.17$.

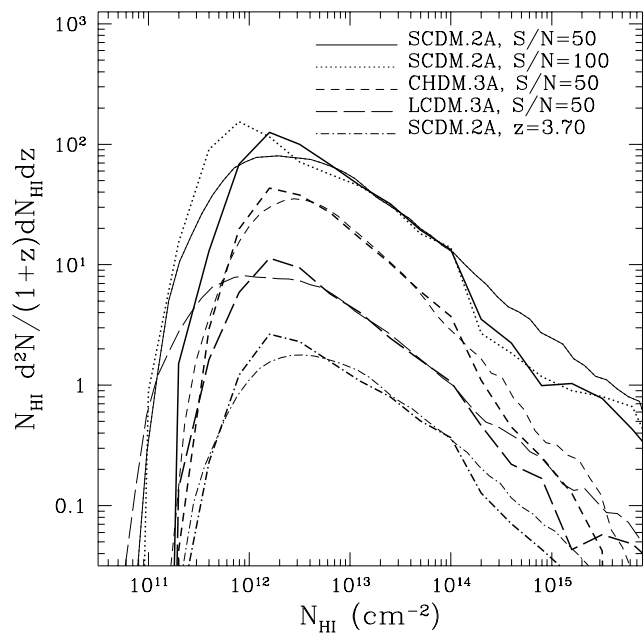


Figure 2. Column density distributions computed using the DPA method (thin lines) and Voigt profile fitting (bold lines) for the SCDM.2A model with $J_{21} = 0.17$ and $S/N = 50$ (solid lines), the SCDM.2A model with $J_{21} = 0.17$ and $S/N = 100$ (dotted lines), the CHDM.3A model with $J_{21} = 0.25$ and $S/N = 50$ (short-dashed lines), the LCDM.3A model with $J_{21} = 0.3$ and $S/N = 50$ (long-dashed lines), and the SCDM.2A model with $J_{21} = 0.25$ and $S/N = 50$ at $z = 3.70$ (dot-dashed lines). The last three models are plotted with the successive vertical offsets of 0.5 dex for clarity.

Table 2. Error budget

Source of error	Slope	Amplitude
HPM is not exact	3%	3%
DPA is not exact	3%	2%
Finite box size	13(3)%	18(5)%
Total error	14(5)%	19(6)%

with the column density distribution from Voigt profile fitting for column densities between about 10^{13} cm^{-2} and 10^{14} cm^{-2} independently of the signal-to-noise ratio in the Voigt profile fitting procedure, but fails at lower and higher column densities. At the lower end, the DPA column density distribution falls off due to the finite resolution of the simulations; in this regime the DPA approximation becomes unreliable, and, at the same time, the Voigt profile fitting technique becomes sensitive to the assumed signal-to-noise ratio in the synthetic spectrum. One can expect, however, that higher resolution (larger mesh size) simulations would improve agreement between the DPA and Voigt profile fitting for lower column densities.

For column densities in excess of 10^{14} cm^{-2} , i.e. for *saturated lines*, the column density distribution computed using Voigt profile fitting shows a feature, while the DPA column density distribution continues as a smooth function of the column density. It is therefore plausible to presume that the feature in the column density distribution obtained by Voigt profile fitting is an artifact of the procedure rather than a change in intrinsic properties of absorbers. However, since all available observational data were analysed using the Voigt profile fitting technique, the same artifact is present in data as well. Thus, it seems reasonable to restrict the range of applicability of the DPA method to column densities between about $10^{12.6} \text{ cm}^{-2}$ and $10^{14.0} \text{ cm}^{-2}$, where the agreement is excellent. As a side note I point out here that this range of column densities is also within the range of applicability of the HPM approximation, which gives accurate results only for overdensities $\delta \lesssim 10$.

2.3 The error budget

The HPM approximation for the hydrodynamics of the low density IGM, combined with the DPA approach, is a powerful and accurate method of computing the column density distribution of unsaturated Lyman-alpha absorption lines. Both approximation, the HPM, and the DPA, are *controlled* approximations, i.e. their range of applicability and their accuracy is well known. It is therefore possible to compute the accuracy with which the column density distribution can be computed using the HPM-DPA combination.

It is now customary to approximate the column density distribution of the Lyman-alpha forest with the power law over a finite range of column densities. Thus, I can convert the error in the computed column density distribution to errors in the amplitude and the slope of the power law. There are three different sources of error in the HPM-DPA calculation, which are summarized in Table 2. First, the HPM itself is not exact. Analysis of Fig. 11 of Gnedin & Hui (1998) shows that the HPM introduces about 3% error to both the slope and the amplitude of the power law. Analysis of Fig.

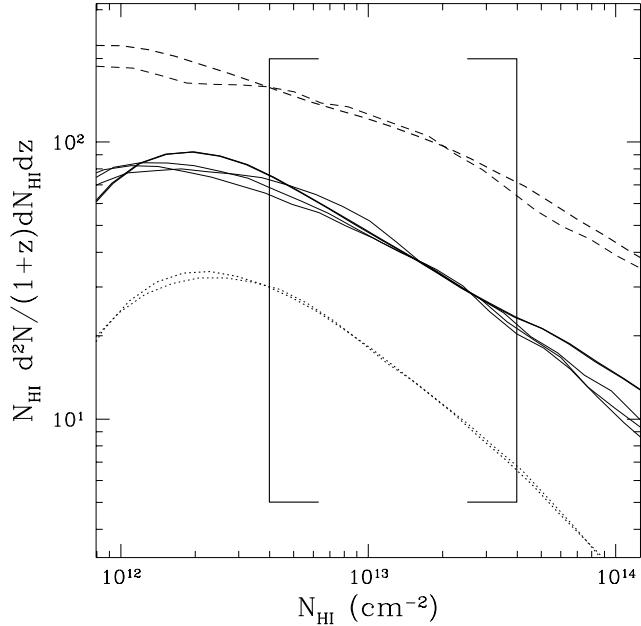


Figure 3. Column density distributions for three variants of the SCDM model: $\sigma_8 = 0.5$ (dotted lines), $\sigma_8 = 0.7$ (solid lines), and $\sigma_8 = 1.2$ (dashed lines). Thin lines show 256^3 simulations and bold lines show 512^3 simulations. For $\sigma_8 = 0.7$ model three different random realization with 256^3 resolution and two different random realizations with 512^3 resolution are shown. The square bracket shows the region where numerical convergence with respect to the box size is achieved. Lines of different type are offset vertically for the sake of clarity.

2 also shows that a 3% error in the slope and a 2% error in the amplitude is introduced by using the DPA instead of Voigt profile fitting for column densities between 10^{13} cm^{-2} and 10^{14} cm^{-2} . Finally, due to the finite size of a computational box, only a subset of all possible initial conditions can be simulated (only one “realization”), and this statistical undersampling also introduces an error. In order to estimate the error due to the realization dependence, I have performed three different realizations of the same cosmological model with the 256^3 mesh and two realizations with the 512^3 mesh (models SCDM.2A, SCDM.2D, and SCDM.2E).

Figure 3 shows column density distributions for all realizations, normalized as explained in §2.4. The difference in slopes and in power law amplitudes for three 256^3 realizations reaches 10% and 18% respectively, while 512^3 simulations have an error a factor of three less in both the slope and the amplitude. Thus, performing 512^3 simulations for all 25 model would substantially reduce the theoretical error, but, as I mention above, since this is beyond the practically possible at the moment, the total error from Table 2 should be properly included in all comparisons between the simulations and the observations.

While Table 2 gives a magnitude of the error, it does not determine the statistical property of this error. In other words, it does not specify what the probability is that a given model would produce results accurate to within the error from Table 2. While there is no simple way to find out the probability distribution of the error, the error in Table 2 should be considered as about 95% confidence interval from

Table 3. Column density limits

Redshift	$\lg(N_{\text{HI,MIN}})$	$\lg(N_{\text{HI,MAX}})$
2.31	12.6	13.2
2.85	12.6	13.6
3.35	13.0	14.0
3.70	13.4	14.0

the way it was computed. This assertion is also supported by comparison between the observations and the simulations in the following section.

2.4 Observational data

I now turn to directly comparing the results of the simulations with the observational data. Recent Keck observations of the Lyman-alpha forest (Hu et al. 1995; Lu et al. 1996; Kirkman & Tytler 1997; Kim et al. 1997) give the column density distribution of the Lyman-alpha forest at four different redshifts: $z = 2.31$, $z = 2.85$, $z = 3.35$, and $z = 3.70$. The data from Kirkman & Tytler (1997) have a median redshift of $z = 2.70$ and about 10% higher amplitude than the data from Hu et al. (1995). Some part of this difference is due to the slightly different redshift of Kirkman & Tytler observations, and some other part (not quite certain at the moment) is due to the Cosmic Variance. But since the current error of my simulations is about 20% in the amplitude, both data samples are consistent with each other for my purpose.

As Fig. 3 also demonstrates, only within a limited range of column densities there is a consistency between 256^3 and 512^3 simulations, i.e. only with this final range a numerical convergence is achieved. Thus, only this range of column densities can be used in comparing observations and simulations. In addition, this range is also a function of redshift, and a figure similar to Fig. 3 at each value of redshift is used to determine the range of column densities at each redshift within which a numerical convergence is achieved. Whenever the range of convergence exceeds the range of applicability of the HPM-DPA approximation, a smaller of two ranges is used (thus maintaining both the accuracy of the HPM-DPA approximation and the numerical convergence of simulations). As can be seen from Fig. 3 the range of convergence is a weak function of the amplitude of the density fluctuations, and thus the same range of column densities can be used for all models.

The specific limits are summarized in Table 3. I only point out here that 512^3 simulations have not been continued beyond $z = 2.85$, and the fitting interval at $z = 2.31$ is determined by extrapolation of fitting intervals at higher redshifts. One thus has to keep in mind that numerical convergence has not been firmly established for simulation results at $z = 2.31$. Therefore, I will only use simulation results at $z = 2.85$, $z = 3.35$, and $z = 3.70$ for quantitative comparison with observations, and will use model predictions at $z = 2.31$ for illustrative purposes only.

For a given range of column densities, I can fit a power law (simultaneously in the slope and amplitude) to both the results of simulations and the observational data. I then fix the amplitude of the column density distribution from

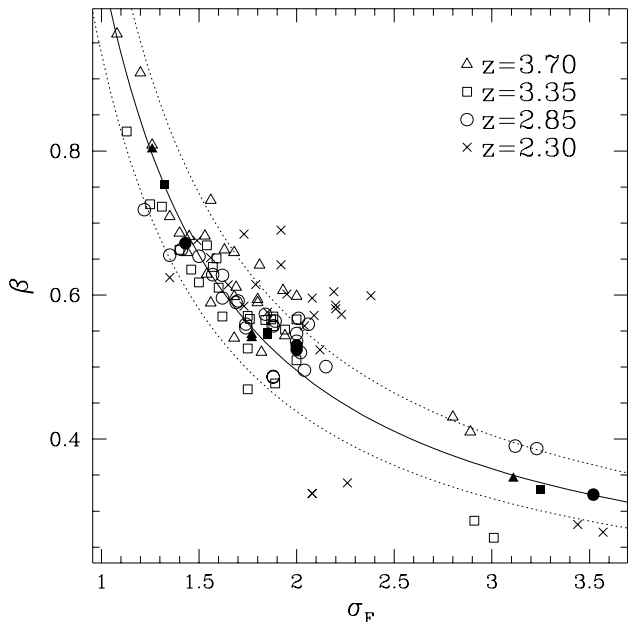


Figure 4. The slope of the column density distribution as a function of the rms linear density fluctuation at the filtering scale σ_F for all models at four different redshifts: $z = 2.31$ (crosses), $z = 2.85$ (circles), $z = 3.35$ (squares), $z = 3.70$ (triangles). Open symbols mark 25 256^3 simulations, and filled symbols show 4 512^3 simulations. The solid line shows the fit 10, and dotted lines show $\pm 13\%$ deviation from the fit.

the simulation by requiring that it coincides with the amplitude fitted to the observational data at the specific value of the column density $N_{\text{HI, FIT}} = 3 \times 10^{13} \text{ cm}^{-2}$ (for all four values of redshift). Thus, for a given simulation this procedure produces two numbers: the slope of the column density distribution β and the amplitude of the column density distribution, which can be expressed as J_{21} . It is the time evolution and the dependence on cosmological parameter of those two quantities that I concentrate on in this paper.

3 RESULTS

3.1 The slope of the column density distribution

I now focus on investigating the dependence of the slope of the column density distribution β on cosmological parameters.

Figure 4 presents the major result of this paper, the dependence of the slope of the column density distribution on the rms linear density fluctuation at the filtering scale. Various open symbols show computed power law slopes for all 25 256^3 models at four different redshifts, and respective solid symbols show four 512^3 models at three highest redshifts. The solid line shows the fit in the form

$$\bar{\beta}(\sigma_F) = \frac{0.76}{\ln(1 + \sigma_F^2)^{0.9}}, \quad (10)$$

and dotted lines mark $\pm 13\%$ interval around the fit (which is consistent with being a 95% confidence interval). I conclude that within the errors of the approximation, the slope of the column density distribution is a function of the rms

linear density fluctuation at the filtering scale alone. This conclusion quantitatively confirms the qualitative conclusion of Hui et al. (1997), who found that more nonlinear models have shallower column density distributions.

The scatter is much smaller for the 512^3 models, as should be expected from Table 2. However, since four 512^3 do not cover the full space of cosmological parameters, they cannot be used to investigate whether the slope of the column density distribution depends on other parameters in addition to σ_F . I however use them to accurately determine the best fit. Fig. 4 thus demonstrates that the slope of the column density distribution of the Lyman-alpha forest β at $N_{\text{HI, FIT}} = 3 \times 10^{13} \text{ cm}^{-2}$ is the function of the density fluctuation on the filtering scale alone to within 13%. It is very likely, judging from how well points from 512^3 simulation fit the solid line, that β is a function of σ_F to much better accuracy (at least 5%), but to verify this requires running several more 512^3 simulations. This work is now in progress.

The scatter around the fit (10) may be caused by two different effects: by the error in the HPM-DPA calculation, and by dependence of the slope β on other cosmological parameters, like the local slope of the power spectrum, the equation of state etc. Because the scatter is consistent with the error alone, current work is not able to address the second source of scatter, i.e. it is possible that the slope of the column density distribution does depend on other parameters of the model, but this dependence is weaker than 13% and therefore cannot be uncovered here. I would like to emphasize that this conclusion does not necessarily contradict the conclusion of Hui et al. (1997), who found a strong dependence of the slope of the column density distribution on both the local slope of the density power spectrum and on the equation of state slope γ . The conclusion of Hui et al. (1997) was based on using a quantity called σ_0 as a measure of the nonlinearity of the model. This quantity is ill-defined, because it measures the amplitude of linear density fluctuation on a scale which is model-dependent and lacks any physical explanation, while σ_F represents to a high degree of accuracy (as have been shown in Gnedin & Hui 1997) the real total (i.e. summed over all scales) rms linear gas density fluctuation. I also note here that since the Zel'dovich approximation used by Hui et al. (1997) is uncontrolled approximation, its accuracy is not known.

I also note here that the scatter around the fit gets larger for higher values of σ_F , as could be expected, as higher σ_F corresponds to more nonlinear models, for which the cosmic variance is more significant. The crosses, which correspond to $z = 2.31$, have a larger scatter, and also somewhat biased toward higher values of β . This is due to the fact that the range of column densities within which numerical convergence is achieved is not established at $z = 2.31$, as have been explained in the previous section. I show the simulation results at $z = 2.31$ here for illustration purposes only; they are not used to determine the fit (10).

Fig. 4 presents the slope β as a function of $\sigma_{F, \text{BOX}}$, because it is $\sigma_{F, \text{BOX}}$, rather than σ_F , which is actually computed in a simulation. But now, given the dependence of the slope β on σ_F , it is possible to correct for this bias, and, given the slope of the column density distribution derived from a simulation, β_{SIM} , to compute the slope β_{COR} which would be derived in an idealistic simulation of an infinite size:

$$\beta_{\text{COR}} = \beta_{\text{SIM}} + \bar{\beta}(\sigma_F) - \bar{\beta}(\sigma_{F,\text{BOX}}), \quad (11)$$

and correct the column density distribution itself accordingly:

$$\frac{N_{\text{HI}} d^2 \mathcal{N}}{(1+z) dz dN_{\text{HI}}} \Big|_{\text{COR}} = \frac{N_{\text{HI}} d^2 \mathcal{N}}{(1+z) dz dN_{\text{HI}}} \Big|_{\text{SIM}} \left(\frac{N_{\text{HI}}}{N_{\text{HI},\text{FIT}}} \right)^{\bar{\beta}(\sigma_F) - \bar{\beta}(\sigma_{F,\text{BOX}})}. \quad (12)$$

where $N_{\text{HI},\text{FIT}} = 3 \times 10^{13} \text{ cm}^{-2}$.

After having corrected for the bias due to the finite simulation size, I can directly compare cosmological models to the observations. Let me first concentrate on $z = 2.85$, since for this value of redshift the HPM-DPA calculation is the most accurate. The observed slope of the column density distribution is $\beta = 0.5$ (Hu et al. 1995; Kirkman & Tytler 1997). However, the error of this number is not quite certain. Therefore, I will say that the model fits the observations if its slope $\bar{\beta}$ is between 0.4 and 0.6 (20% total [15% observational plus 13% modeling] error); if the slope of the column density distribution for a model falls between 0.35 and 0.40 or between 0.60 and 0.65 (30% total error), I will say that the model marginally fits the data; finally, if the slope β for a given model is above 0.65 or below 0.35, I will assume that the model fails.

Table 4 presents the biased β_{SIM} and corrected β_{COR} values for the slope of the column density distribution for all *COBE* normalized models from Table 1, as well as the value of $\bar{\beta}$ computed from equation (10). The cosmological parameters for the models are included for reference. Finally, the last column indicates whether the model fits the data (+), marginally fits (\pm), or fails completely (-).

Finally, using equation (10), it is possible to place a constraint on the value of the rms linear density fluctuation σ_F . The observational constraint $0.4 < \beta < 0.6$ can be expressed in terms of σ_F as

$$1.6 < \sigma_F < 2.6. \quad (13)$$

This should be considered as roughly 2σ (95% confidence level) interval. With the 3σ error, this interval becomes

$$1.5 < \sigma_F < 3.1.$$

The median value, $\beta = 0.5$ corresponds to $\sigma_F = 2.0$.

Finally, as I have mentioned in the previous section, the filtering scale $1/k_F$ depends on reionization history and is a nontrivial function of time. For a purpose of a quick estimate, it would be more convenient to use a fixed scale like $1/k_{34}$ (eq. [6]). The following approximate expression accurate to about 5% can then be used to compute σ_F at $z = 2.85$ from σ_{34} :

$$\sigma_F(z = 2.85) = \sigma_{34} [1.06 - 0.9(\gamma - 1.5) - 0.15(T_4 - 1)].$$

This expression depends on the parameters of the equation of state since σ_F depends on the equation of state while σ_{34} does not. I point out here that the above expression is derived by analyzing 25 models considered in this paper, and may not be valid for a model that falls outside the range of cosmological models considered here, or for a model whose equation of state evolves significantly differently from the analytical expressions of Hui & Gnedin (1998).

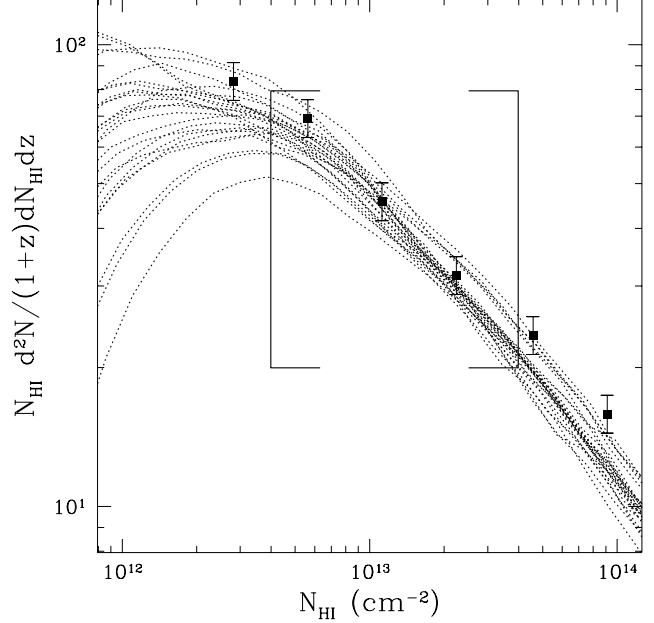


Figure 5. Comparison between the observational data at $z = 2.85$ and all 25 cosmological models, reduced to have the slope of the column density distribution of 0.5 (eq. [15]) and normalized according to equation 14 (dotted lines).

3.2 The amplitude of the column density distribution

While the slope of the column density distribution can serve as a basis for discriminating against some of the cosmological models, the amplitude of the column density distribution depends on the assumed value for the ionizing intensity J_{21} , which is currently highly uncertain. The best available measurements are based on the proximity effect, and give values in the range $J_{21} = 0.2 - 1.5$ at $z = 2 - 4$ (Giallongo et al. 1996; Lu et al. 1996; Cooke, Espey, & Carswell 1997). I therefore consider J_{21} as a free parameter, and use the observational data to fix the value for J_{21} that best fits the data.

Let me first consider $z = 2.85$. The normalization procedure described in the previous subsection defines a value of J_{21} for each cosmological model. After computing the respective J_{21} values for all 25 models, I obtain the following *approximate* expression for J_{21} as a function of cosmological parameters:

$$J_{21}(z = 2.85) = 10^3 \frac{\Omega_b^2 h^3}{\Omega_0^{1/2} T_4^{0.7} \sigma_F}, \quad (14)$$

which is accurate to about 40%. The accuracy estimate results from the assumed accuracy of 20% for the amplitude of the column density distribution, which in turn translates into a 40% accuracy in $J_{21} \propto N_{\text{HI}}$ for the power-law column density distribution with the index $\beta \approx 0.5$.

In order to demonstrate graphically the level of accuracy of this approximation, I plot all 25 models with the value of J_{21} defined according to equation (14), “reduced” to have the same slope of the column density distribution,

$$\frac{N_{\text{HI}} d^2 \mathcal{N}}{(1+z) dz dN_{\text{HI}}} \Big|_{\text{RED}} \equiv$$

Table 4. Models vs observations

Model	Ω_0	Ω_b	Ω_Λ	Ω_ν	h	n	σ_8	β_{SIM}	β_{COR}	$\bar{\beta}$	fit?
SCDM.5A ^a	1	0.05	0	0	0.5	1	1.2	0.33	0.32	0.30	–
TCDM.2A	1	0.05	0	0	0.5	0.9	0.83	0.57	0.51	0.48	+
LCDM.1A	0.35	0.05	0.65	0	0.7	1	0.94	0.59	0.51	0.51	+
LCDM.1C	0.35	0.05	0.65	0	0.7	1	0.94	0.56	0.52	0.44	+
LCDM.2A	0.35	0.05	0.65	0	0.7	0.96	0.80	0.63	0.56	0.55	+
LCDM.3A	0.35	0.03	0.65	0	0.7	1	1.04	0.57	0.51	0.44	+
LCDM.4A	0.35	0.03	0.65	0	0.7	0.95	0.85	0.65	0.56	0.58	+
LCDM.5A	0.4	0.036	0.6	0	0.65	1	1.02	0.54	0.48	0.44	+
CHDM.1A	1	0.05	0	0.1	0.5	1	0.92	0.52	0.47	0.44	+
CHDM.2A	1	0.05	0	0.15	0.5	1	0.86	0.63	0.54	0.56	+
CHDM.3A	1	0.05	0	0.2	0.5	1	0.82	0.72	0.57	0.73	–
CHDM.4A	1	0.05	0	0.1	0.65	1	1.22	0.39	0.37	0.31	–
CHDM.5A	1	0.05	0	0.2	0.65	1	1.12	0.56	0.49	0.46	+
CHDM.6A	1	0.07	0	0.1	0.6	0.9	0.73	0.66	0.56	0.63	±

^a A 512^3 simulation is used for this model.

$$\left. \frac{N_{\text{HI}} d^2 \mathcal{N}}{(1+z) dz dN_{\text{HI}}} \right|_{\text{SIM}} \left(\frac{N_{\text{HI}}}{N_{\text{HI, FIT}}} \right)^{0.5 - \bar{\beta}(\sigma_{F, \text{BOX}})} \quad (15)$$

In other words, if both equation (10) and equation (14) were exact, the reduced column density distribution would be the same for all cosmological models. Thus, the difference between different lines in Fig. 5 demonstrates the error in both equation (10) and equation (14).

One can note that while the majority of models lie together in a strip coinciding with the data points, there are six models (SCDM.2D, SCDM.2G, SCDM.2H, SCDM.2L, LCDM.1C and LCDM.2A) that lie above the rest. This difference correlates with neither of the cosmological parameters defining the model. More than that, since one of the outliers (SCDM.2D) is just a different random realization of the SCDM.2A model, the difference in the amplitude is real, and is due to the error induced by the HPM-DPA approximation, most likely the finite size of a simulation box. One therefore may hope that the dispersion in Fig. 5 can be reduced by using larger simulation sizes (work currently in progress).

Finally, I would like to point out here that Ω_b and h dependence in equation (14) agrees with the one obtained by Croft et al. (1996) when the dependence of T_0 on Ω_b (for a given cosmological model) is taken into account (Hui & Gnedin 1998). However, the advantage of equation (14) is that it is (approximately) valid for *any* cosmological model, i.e. there exist no additional dependences on physical parameters that are not incorporated into equation (14), except at a level comparable to or below the error of the HPM-DPA calculation.

I note here, that since both T_0 and σ_F are non-trivial functions of time, and it is unlikely that $z = 2.85$ represents a special moment in the history of the universe, equation (14) cannot hold at some other redshift with the coefficient 10^3 being replaced by some other appropriate number. In other words, while it is plausible that the expression (10) for the slope of the column density distribution is accurate to high precision, equation (14) is *necessary approximate*, and there *has* to be some other dependence in equation (14) on cosmological parameters at the 40% or below level.

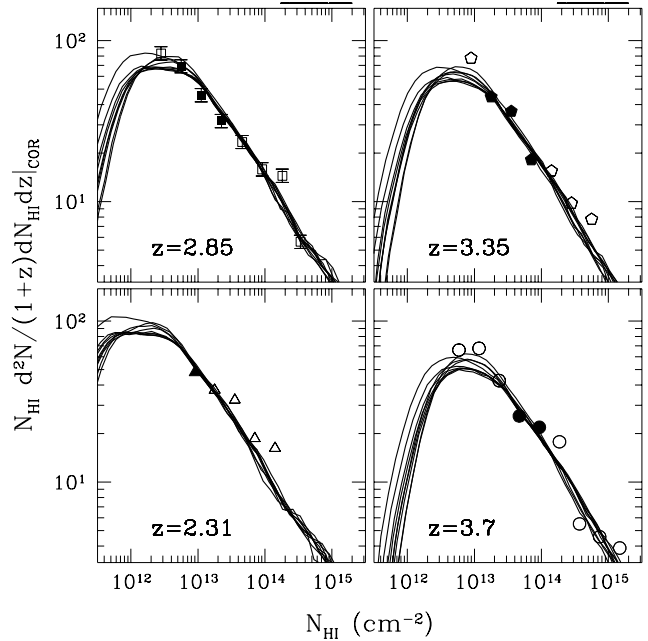


Figure 6. Comparison between the models that fit the data at $z = 2.85$ and observations at four different redshifts. The same value of J_{21} is adopted for each cosmological model at all four redshifts. Symbols show the observational data with solid symbols lying in the column density range used to fit the amplitude of the column density distribution.

3.3 The evolution of the column density distribution

Using the observational data at four different redshifts, it is possible to constraint the evolution of the column density distribution of the Lyman-alpha forest from $z \sim 4$ to $z \sim 2$.

I show in Figure 6 the column density distributions for the seven models from Table 4 that fit the data at all four redshifts. For every model the value of J_{21} is the same at each redshift (but different for different models). Since all models are consistent with the data at all four redshifts, the observations are consistent with the value of J_{21} being

independent of redshift in the redshift interval $z \sim 2 - 4$. This normalization is also fully consistent with the slightly higher abundance of the Lyman-alpha forest absorbers at $z \approx 3$ found by Kirkman & Tytler (1997) within the errors of the analysis presented in this paper.

4 DISCUSSION

I have demonstrated that the slope of the column density distribution of the Lyman-alpha forest is a function of the rms linear density fluctuation of the gas distribution (which is smooth on scales below the characteristic filtering scale), and is independent of other cosmological parameters within the accuracy of about 13% of the approximate method utilized (Hydro-PM approximation combined with the Density-Peak Ansatz). The amplitude of the column density distribution, expressed in terms of the ionizing intensity J_{21} , is proportional to a combination of cosmological parameters,

$$J_{21} \propto \frac{\Omega_b^2 h^3}{\Omega_0^{1/2} T_{4.7}^{0.7} \sigma_F},$$

and is independent of other cosmological or physical parameters within about 40% accuracy, at a given value of redshift.

The observational data and the modeling technology are currently consistent with the value of J_{21} being constant from $z \sim 4$ until $z \sim 2$.

In order for a cosmological model to fit the observed slope of the column density distribution of the Lyman-alpha forest at $z \approx 3$, the rms linear density fluctuation at the filtering scale $k_F \sim k_{34}$ (see eq. [6]) in the model should be between 1.6 and 2.6 (or between 1.5 and 3.1 with a conservative estimate).

Why is the rms linear density fluctuation the major factor determining the slope of the column density distribution, when $\sigma_F \sim 2$ means an already nonlinear distribution? The answer is that σ_F serves as a measure of the nonlinearity of the model; one could have adopted another measure, say, the total (nonlinear) rms density fluctuation in the model. However, since the total rms density fluctuation is a function of the rms linear density fluctuation (Kofman et al. 1994) with, perhaps, a slight dependence on the local value of the slope of the density power spectrum, which is within the uncertainty of the simulations presented here, any measure of the nonlinearity of the model can be expressed as a function of σ_F .

Finally, a few comments can be made about fitting a cosmological model to the observational data. If one ignores semi-philosophical questions about the Hubble constant, the age of the universe, and the value of Ω_0 , and restricts oneself to requiring that a given cosmological model satisfy three measurements of the underlying density power spectrum: the *COBE* normalization, the cluster abundance, and the slope of the column density distribution of the Lyman-alpha forest at $z \approx 3$, once can then ask a question how well the cosmological models listed in Table 1 would perform on those three tests. Let me concentrate only on the models that pass the first test, i.e. only on the *COBE* normalized models listed in Table 4. Using the fit $\sigma_{8, \text{CLUSTER}}$ for the top-hat linear density fluctuation at the $8h^{-1}$ Mpc scale that satisfies the cluster constraint from Eke, Cole, & Frenk (1996),

$$\sigma_{8, \text{CLUSTER}} = (0.50 \pm 0.04) \Omega_0^{-0.53+0.13\Omega_0},$$

I compute the error in the amplitude of the linear density fluctuation at the cluster scale,

$$\frac{\sigma_8}{\sigma_{8, \text{CLUSTER}}} - 1.$$

The error in the slope of the column density distribution of the Lyman-alpha forest (assuming the observations give $\beta = 0.5$) is simply

$$\frac{\beta}{0.5} - 1.$$

Table 5 lists all fourteen models together with the respective errors in the density fluctuation amplitude at the cluster scale and in the slope of the column density distribution of the Lyman-alpha forest (the check mark after the error shows whether the model passes the test at a 95% confidence level or not). One can see that many models do well. Several of LCDM models pass all three tests. The fact that none of the CHDM models presented pass all the tests does not imply that this model can be ruled out: it seems plausible that a set of parameters can be found that will satisfy all three tests. The set of CHDM models used in this paper has been chosen “randomly”, without prior attempts to make these models fit the cluster abundance and the slope of the column density distribution tests. The fact that several of “randomly” chosen LCDM models perform well implies that there is more parameter space available for the LCDM models than for CHDM models, but it will be premature to claim that CHDM model fail altogether.

It however seems possible to make a claim that the density parameter in massive neutrinos, Ω_ν , has to be lower than or about 0.15. The two models, CHDM.3A and CHDM.5A, represent two extreme cases of the $\Omega_\nu = 0.2$ models, and they clearly demonstrate that models with $\Omega_\nu = 0.2$ have too little power on scales of about 100 kpc as compared with 10 Mpc scales.

I am very grateful to Romeel Dave for letting me use his AUTOVP automated Voigt profile fitting software. This work was supported by the UC Berkeley grant 1-443839-07427. Simulations were performed on the NCSA Power Challenge Array under the grant AST-960015N and on the NCSA Origin2000 mini super-computer under the grant AST-970006N.

REFERENCES

- Arons, J. 1972, ApJ, 172, 553
- Bahcall, J. N., Salpeter, E. E. 1965, ApJ, 142, 1677
- Bi, H. G., Borner, G., Chu, Y. 1992, A&A, 266, 1
- Bi, H. G., Davidsen, A. F. 1997, ApJ, 479, 523
- Black, J. H. 1981, MNRAS, 197, 553
- Bond, J. R., Szalay, A. S., Silk, J. 1988, ApJ, 324, 627
- Bunn, E. F., White, M. 1997, ApJ, 480, 6
- Cen, R. Y., Miralda-Escudé, J., Ostriker, J. P., Rauch, M. R. 1994, ApJ, 437, L9
- Cooke, A. J., Espey, B., Carswell, B. 1997, MNRAS, 284, 552
- Cristiani, S., D’Odorico, S., D’Odorico, V., Fontana, A., Galongo, E., & Savaglio, S. 1998, MNRAS, in press (astro-ph 9610006)
- Croft, R. A. C., Weinberg, D. H., Katz, N., Hernquist, L. 1996, ApJ, 488, 532
- Dave, R., Hernquist, L., Weinberg, D. H., Katz, N. 1997, ApJ, 477, 21

Table 5. COBE normalised models

Model	Ω_0	Ω_b	Ω_Λ	Ω_ν	h	n	σ_8	$\frac{\sigma_8}{\sigma_{8,CLUSTER}} - 1$	$\frac{\beta}{0.5} - 1$	
SCDM.5A	1	0.05	0	0	0.5	1	1.20	+140%	-40%	
TCDM.2A	1	0.05	0	0	0.5	0.9	0.83	+66%	-4%	✓
LCDM.1A	0.35	0.05	0.65	0	0.7	1	0.94	+13%	+2%	✓
LCDM.1C	0.35	0.05	0.65	0	0.7	1	0.94	+13%	-12%	✓
LCDM.2A	0.35	0.05	0.65	0	0.7	0.96	0.80	-4%	+10%	✓
LCDM.3A	0.35	0.03	0.65	0	0.7	1	1.04	+25%	+12%	✓
LCDM.4A	0.35	0.03	0.65	0	0.7	0.95	0.85	+2%	+16%	✓
LCDM.5A	0.4	0.036	0.6	0	0.65	1	1.02	+32%	-12%	✓
CHDM.1A	1	0.05	0	0.1	0.5	1	0.92	+84%	-12%	✓
CHDM.2A	1	0.05	0	0.15	0.5	1	0.86	+72%	+46%	
CHDM.3A	1	0.05	0	0.2	0.5	1	0.82	+64%	+64%	
CHDM.4A	1	0.05	0	0.1	0.65	1	1.22	+144%	-38%	
CHDM.5A	1	0.05	0	0.2	0.65	1	1.12	+124%	-8%	✓
CHDM.6A	1	0.07	0	0.1	0.6	0.9	0.73	+46%	+26%	

- D'Odorico, V., Cristiani, S., D'Odorico, S., Fontana, A., Giallongo, E. 1998, A&A, in press
- Doroshkevich, A. G. Shandarin, S. 1977, MNRAS, 179, 95
- Eke, V. R., Cole, S., Frenk, C. S. 1996, MNRAS, 282, 263
- Giallongo, E., Cristiani, S., D'Odorico, S., Fontana, A., Savaglio, S. 1996, ApJ, 466, 46
- Gnedin, N. Y., Hui, L. 1996, ApJ, 472, L73
- Gnedin, N. Y., Hui, L. 1998, MNRAS, in press (astro-ph 9706219)
- Hernquist, L., Katz, N., Weinberg, D. H., Miralda-Escudé, J. 1996, ApJ, 457, L51
- Hu, E., Kim, T., Cowie, L. L., Songaila, A. 1995, AJ, 110, 1526
- Hu, W., Sugiyama, N. 1996, ApJ, 471, 542
- Hui, L., Gnedin, N. Y. 1998, MNRAS, in press (astro-ph 9612232)
- Hui, L., Gnedin, N. Y., Zhang, Y. 1997, ApJ, 486, 599
- Ikeuchi, S. 1986, ApSS, 118, 509
- Ikeuchi, S., Ostriker, J. P. 1986, ApJ, 301, 522
- Kim, T., Hu, E. M., Cowie, L. L., Songaila, A. 1997, AJ, 114, 1
- Kirkman, D., Tytler, D. 1997, ApJ, 484, 672
- Kofman, L. A., Bertschinger, E., Gelb, J. M., Nusser, A., Dekel, A. 1994, ApJ, 420, 44
- Lu, L., Sargent, W. L. W., Womble, D. S., Takada-Hidai, M. 1996, ApJ, 472, 509
- Ma, C.-P. 1996, ApJ, 471, 13
- McGill, C. 1990, MNRAS, 242, 544
- Miralda-Escudé, J., Cen, R., Ostriker, J. P., Rauch, M. 1996, ApJ, 471, 582
- Mücket, J. P., Petitjean, P., Kates, R. E., Riediger, R. 1996, A&A, 301, 417
- Ostriker, J. P., Ikeuchi, S. 1983, ApJ, 268, L63
- Petitjean, P., Mücket, J. P., Kates, R. E. 1995, A&A, 295L, 9
- Rauch, M., Miralda-Escudé, J., Sargent, W. L. W., Barlow, T., Weinberg, D. H., Hernquist L., Katz N., Cen R., Ostriker J. P. 1997, ApJ, 489, 7
- Rees, M. J. 1986, MNRAS, 218, 25
- Rees, M. J. 1988, in QSO Absorption Lines, ed. J. C. Blades, D. A. Turnshek, C. A. Norman (Cambridge: Cambridge Univ. Press)
- Wadsley, J. W., Bond, J. R. 1997, PASP Conf. Ser. 123, 332
- Weinberg, D. H., private communication
- Weinberg, D. H., Miralda-Escudé, J., Hernquist, L., Katz, N. 1998, ApJ, in press (astro-ph 9701012)
- Zhang, Y., Anninos, P., Norman, M. L. 1995, ApJ, 453, L57
- Zhang, Y., Anninos, P., Norman, M. L., Meiksin, A. 1997, ApJ, 485, 496 (astro-ph 9609194)